Journal of Advanced Research 65 (2024) 197–210

Contents lists available at ScienceDirect

Journal of Advanced Research

journal homepage: www.elsevier.com/locate/jare

SIRT1, a target of *miR-708-3p*, alleviates fluoride-induced neuronal damage via remodeling mitochondrial network dynamics

Qian Zhao [a,b,c], Guo-yu Zhou [a,b,d], Qiang Niu [a,b], Jing-wen Chen [a,b], Pei Li [a,b], Zhi-yuan Tian [a,b], Dong-jie Li [a,b], Tao Xia [a,b,*], Shun Zhang [a,b], Ai-guo Wang [a,b,*]

[a] *Department of Occupational and Environmental Health, School of Public Health, Tongji Medical College, Huazhong University of Science and Technology, Wuhan, Hubei, People's Republic of China*
[b] *Key Laboratory of Environment and Health, Ministry of Education & Ministry of Environmental Protection, State Key Laboratory of Environmental Health (incubating), School of Public Health, Tongji Medical College, Huazhong University of Science and Technology, Wuhan, Hubei, People's Republic of China*
[c] *Department of Toxicology, School of Public Health, Shanxi Medical University, Taiyuan, Shanxi, People's Republic of China*
[d] *Department of Environmental Health, College of Public Health, Zhengzhou University, Zhengzhou, Henan, People's Republic of China*

HIGHLIGHTS

- SIRT1 activation exerted protective roles against fluoride-induced cognitive defects.
- SIRT1 activation restored fluoride-caused defective mitochondrial network dynamics.
- SIRT1 was targeted directly by *miR-708-3p*.
- *MiR-708-3p* mediated the neurotoxic process of fluoride via directly targeting SIRT1.
- SIRT1, a target of *miR-708-3p*, alleviates fluoride-induced neuronal damage via remodeling mitochondrial network dynamics.

GRAPHICAL ABSTRACT

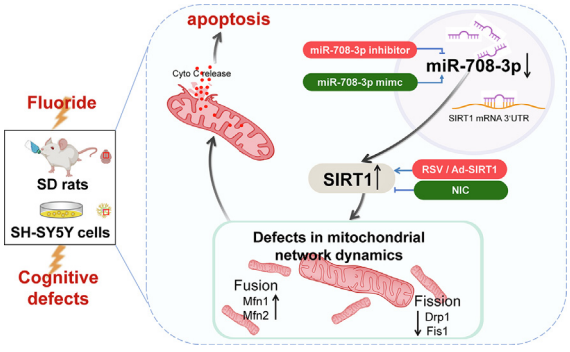

ARTICLE INFO

Article history:
Received 30 August 2023
Revised 23 November 2023
Accepted 26 November 2023
Available online 28 November 2023

Keywords:
SIRT1
miR-708-3p
Fluoride
Neuronal damage
Mitochondrial network dynamics

ABSTRACT

Introduction: Neurological dysfunction induced by fluoride contamination is still one of major concern worldwide. Recently, neuroprotective roles of silent information regulator 1 (SIRT1) focusing on mitochondrial function have been highlighted. However, what roles SIRT1 exerts and the underlying regulative mechanisms, remain largely uncharacterized in such neurotoxic process of fluoride.
Objectives: We aimed at evaluating the regulatory roles of SIRT1 in human neuroblastoma SH-SY5Y cells and Sprague-Dawley rats with fluoride treatment, and to further identify potential miRNA directly targeting SIRT1.
Methods: Pharmacological suppression of SIRT1 by nicotinamide (NIC) and promotion of SIRT1 by adenovirus (Ad-SIRT1) or resveratrol (RSV) were employed to assess the effects of SIRT1 in mitochondrial dysfunction induced by fluoride. Also, miRNAs profiling and bioinformatic prediction were used to screen the miRNAs which can regulate SIRT1 directly. Further, chemical mimic or inhibitor of chosen miRNA was applied to validate the modulation of chosen miRNA.
Results: NIC exacerbated defects in mitochondrial network dynamics and cytochrome *c* (Cyto C) release-driven apoptosis, contributing to fluoride-induced neuronal death. In contrast, the ameliorative effects were observed when overexpressing SIRT1 by Ad-SIRT1 *in vitro* or RSV *in vivo*. More importantly, *miR-708-3p* targeting SIRT1 directly was identified. And interestingly, moreover, treatment with chemically

* Corresponding authors at: Department of Occupational and Environmental Health, School of Public Health, Tongji Medical College, Huazhong University of Science and Technology, Wuhan, Hubei, People's Republic of China.
E-mail addresses: xiaotao1988@hust.edu.cn (T. Xia), wangaiguo@mails.tjmu.edu.cn (A.-g. Wang).

https://doi.org/10.1016/j.jare.2023.11.032

modified *miR-708-3p* mimic aggravated, while *miR-708-3p* inhibitor suppressed fluoride-caused neuronal death. Further confirmedly, overexpressing SIRT1 effectively neutralized *miR-708-3p* mimic-worsened fluoride neuronal death via correcting mitochondrial network dynamics. On contrary, inhibiting SIRT1 counteracted the promotive effects of *miR-708-3p* inhibitor against neurotoxic response by fluoride through aggravating abnormal mitochondrial network dynamics.

Conclusion: These data underscore the functional importance of SIRT1 to mitochondrial network dynamics in neurotoxic process of fluoride and further screen a novel unreported neuronal function of *miR-708-3p* as an upstream regulator of targeting SIRT1, which has important theoretical implications for a potential therapeutic and preventative target for treatment of neurotoxic progression by fluoride.

Introduction

Neurological disorders and cognitive defects affect a significant part of population [1]. Impairments to cognition often result from a number of factors including environmental neurotoxicants, gene defects, adult related diseases, and so on [2]. Strikingly, fluoride is not only widely distributed in the environment but also extensively used in industrial settings and the injurious effects of environmental fluoride contamination on neurons have been gaining much attention, as fluoride acts as a double-edged sword turning out more injurious to public health than being beneficial [3,4]. Hitherto, multisite studies have shown that long-term consumption of excessive fluoride exerts negative impact on cognitive capacities of rats [5,6] and is a potential risk factor for cognitive impairment among residents in fluorosis areas [7], indicating an urgent need for studies identifying innovative therapeutic and preventative strategies.

Silent information regulator 1 (SIRT1), highly expressed in neurons, is a predominant protein that has been shown to play a role in the neuroprotective effects through multiple mechanisms [8]. In particular, the protective potentials of SIRT1 through regulation of mitochondrial function during neurological disorders have been emphasized in many studies published in recent years [9]. Currently, under the condition of neuronal injuries by fluoride, some of achievements have been done concerning the interaction of SIRT1 with mitochondria. Results in our previous studies showed that SIRT1 restoration activated mitochondrial p53 pathway to resist fluoride-induced neurological damage [10]. Along with the aforesaid mitochondrial damages caused by fluoride, defects in mitochondrial fusion/fission dynamics were also identified, as manifested by facilitating fusion proteins mitofusion 1 (Mfn1), mitofusion 2 (Mfn2) and suppressing fission proteins dynamin-related protein 1 (Drp1), fission 1 (Fis1) [11]. Undoubtedly, extensive remodeling of mitochondrial network dynamics, involving mitochondrial fusion/fission dynamics as well as ultrastructural remodeling of mitochondria, is essential for mitochondrial homeostasis and diseases often manifest if disturbed [12]. However, whether SIRT1 interacts with mitochondrial network dynamics under fluoride-injured neuronal death has not been clearly investigated.

microRNAs (miRNAs) are versatile regulators of gene expression, instigating tremendous interest in researches [13]. Recently, the great expansion of understanding about the function of miRNAs and also their roles in the modulation of SIRT1 have provided a distinctive vision in the mechanisms of neuronal injuries [14]. To date, several miRNAs, such as *miR-34a* and *miR-9*, have been shown to negatively modulates SIRT1 contributing to neural differentiation [15,16]. Especially, alterations of miRNAs levels have been shown in fluoride-exposed various tissues [17,18]. Nonetheless, till now, only levels of *miR-125b*, *miR-124* and *miR-132* were elevated in hippocampi of mice with fluoride treatment [19], little is known about whether miRNAs are responsible for altered SIRT1 levels induced by fluoride.

Therefore, in this study, using neuronal defects established by *in vitro* SH-SY5Y cell culture and *in vivo* Sprague-Dawley rat model of fluoride exposure, the potential roles of SIRT1 and the underlying regulative mechanisms were assessed. More importantly, we also aimed at exploring the miRNAs targeting SIRT1 and its modulations in neurotoxic process of fluoride.

Material and methods

Reagents

Sodium fluoride (NaF, #S7920), resveratrol (RSV, #5010) and nicotinamide (NIC, #47865-U) were obtained from Sigma-Aldrich Co. (St Louis, MO, USA). *miR-708-3p* mimic, *miR-708-3p* inhibitor and corresponding negative control (NC), miRcute miRNA Isolation Kit (#DP501), and miRcute Plus miRNA qPCR Kit (#FP411) were obtained from TIANGEN Biotech Co. (Beijing, China). DMEM/Ham's F-12 (#C11330) and fetal bovine serum (FBS, #10099141) were purchased from Thermo Fisher Scientific Inc. (Altham, Massachusetts, USA). JC-10, MitoTracker Red CMXRos probe (#M7512), TRIzol reagent (#15596–026) and lipofectamine RNAiMax Transfection Reagent (#13778–150) was purchased from Invitrogen Corp. (Carlsbad, CA, USA). Polyvinylidene fluoride membrane (PVDF, #03010040001) and *In Situ* Cell Death Detection Kit (fluorescein) (#11684795910) were purchased from Roche Inc. (Nutley, New Jersey, USA). Primary antibodies against SIRT1 (#13161–1-AP), cytochrome *C* (Cyto C, #10993–1-AP), Mfn2 (#12186–1-AP), Fis1 (#10956–1-AP) and horseradish peroxidase-conjugated anti rabbit/mouse secondary antibodies were obtained from Proteintech Inc. (Wuhan, China). Primary antibodies against cleaved poly ADP-ribose polymerase (PARP, #9542S) and cleaved caspase-3 (#9664S) were obtained from Cell Signaling Technology Inc. (Beverly, MA, USA). Primary antibodies against Mfn1 (#ab57602) and Drp1 (#ab56788) were obtained from Abcam Inc. (Cambridge, MA, USA). Primary antibody against GAPDH (#AP0063) was obtained from Bioworld Technology Inc. (St Louis Park, MN, USA). ECL reagent (#K-12049-D50) was obtained from Advansta Inc. (Menlo Park, CA, USA). Annexin V-fluorescein isothiocyanate (FITC) and Propidium iodine (PI) staining kit (#556547) was purchased from BD Biosciences. (San Jose, CA, USA). Cell Counting Kit-8 (CCK-8, #CK04), Nissl detection kit, Alexa Fluor 488 goat anti-mouse IgG (H + L) and Alexa Fluor 488 AffiniPure goat anti-mouse/rat IgG (H + L) were purchased from Promoter Biotechnology. (Wuhan, China). Revert Aid First Strand cDNA Synthesis Kit (#K1621) were purchased from Fermentas Inc. (Hanover, MD, USA).

Cell culture and chemical treatments

Human neuroblastoma SH-SY5Y cells, from American Type Culture Collection (ATCC Inc., Manassas, VA, USA) were cultured in DMEM/Ham's F-12 supplemented with 10 % FBS. HEK293T cells were obtained from ATCC and cultured in DMEM supplemented with 10 % FBS. All cells were cultured in a humidified atmosphere containing 5 % CO_2 at 37°C. When reaching 70–80 % confluence,

SH-SY5Y cells were subjected to NaF (60 mg/L) or NIC (3 mM) for 24 h.

Adenoviral transfection

SH-SY5Y cells were transfected with adenoviruses harboring SIRT1 (Ad-SIRT1). The titers of Ad-SIRT1 were 1.2×10^{10} PFU/mL, and MOI was 200:1. Cells were subjected to NaF for 24 h after 24 h-long adenoviral transfection.

Western blotting

Protein samples were extracted from cells and neuronal tissues (hippocampi and striata). Protein detections were performed using primary antibodies recognizing SIRT1 (1:1000), Cyto C (1:500), cleaved PARP (1:500), cleaved caspase-3 (1:500), Mfn1 (1:1000), Mfn2 (1:1000), Drp1 (Abcam Inc., 1:2000), Fis1 (1:1000), and GAPDH (1:8000). Then, antigen-primary antibody complexes were incubated with secondary antibodies and visualized using ECL reagents for chemiluminescent reading on a GeneGnome chemiluminescent imaging system (Syngene Inc., Frederick, MD, USA). Intensity values of target bands were normalized to GAPDH and quantified using the Quantity One software (Bio-Rad, Hercules, CA, USA).

Cell viability assay

For cell viability assay, the number of cells with various treatments were assessed using CCK-8. Synergy 4 multifunctional microplate reader (BioTek Instruments Inc., Winooski, VT, USA) was employed for absorbance measurements. Results were showed as the percentage of values of the Control set as 100 %.

Flow cytometry

After corresponding treatments, cells undergoing apoptosis were distinguished from live and necrotic cells by using Annexin V- FITC (5 μL) and PI (5 μL) staining kit. Treated cells were resuspended with JC-10 working solution (20 μM) for mitochondrial membrane potential (MMP).

Confocal laser microscopy

Mitochondrial morphology was observed in SH-SY5Y cells stained with MitoTracker Red CMXRos probe (100 nM, 30 min at 37°C). To observe the co-localization of Cyto C with mitochondria, cells with mitochondrial staining were routinely fixed, permeabilized, blocked, and incubated with primary antibodies against Cyto C (1:500, at 4°C overnight). Then, after Alexa Fluor 488 goat anti-mouse IgG (H + L) incubation (1:500, 1 h at 37°C), cell nuclei were stained with DAPI and fluorescent signals were imaged under the laser scanning confocal microscope (Olympus Co., Tokyo, Japan).

Animal experiments

In order to imitate environmental fluoride levels in drinking water, fluoride rat model was established following previous reports [20]. In brief, female rats were randomly divided into 4 groups. Control rats received tap water in which fluoride ion is less than 1.0 mg/L. The rats from other groups were given a free drink of drinking water supplemented with 10, 50 and 100 mg/L NaF (corresponding to 4.52, 22.6 and 45.2 mg/L fluoride ion, respectively), for 6 consecutive months (Fig. S2A). For SIRT1 interference, rats were treated with RSV (200 mg/kg, through gavage) or NIC (100 mg/kg, through gavage) respectively for 60 consecutive days. The dosage of RSV or NIC treatment was chosen base on previous studies [20]. The treatment schedules were shown in Fig. 3A. At the end of the experiments, hippocampi and striata were collected.

Ethics statements

All rat experiments were carried out in accordance with the Guidelines for the Care and Use of Laboratory Animals published by Ministry of Health People's Republic of China and approved by the Ethics Review Committee for Animal Research at Huazhong University of Science and Technology (Approval No. HUST NY/MA-029–2018).

Neurobehavior assays

Morris water maze test was performed [11]. Briefly, rats were trained to find a submerged platform in an open circular swimming arena with dark walls and dark opaque water. The arena was conditionally divided into 4 quadrants and the platform was fixed at the center of one quadrant. Repeated trials were performed each day by placing rats into water at the start location of each quadrant. Each trial lasted 60 s with an additional 15 s learning time where rats were allowed to remain on the platform. After 4 days of learning, rats were subjected to a spatial probe test where platform was removed. Rats were analyzed for number of times they passed through the previous platform site and the proportion of swimming distance and time they spent in the platform quadrant. All behavior data of rats in the swimming arena was recorded by a video camera connected to a digital tracking device, which was attached to a computer with water maze software (Electric factory of Wuhan, Hubei, China).

Immunostaining

Samples from hippocampi and striata were harvested, fixed with paraformaldehyde, and embedded in paraffin. To quantify Nissl bodies in Neurons, Nissl staining was performed using a Nissl detection kit. Slices for immunohistochemical (IHC) and immunofluorescent staining were firstly blocked for nonspecific binding sites. For immunoreactivities of SIRT1 and mitochondrial fusion/fission dynamics proteins, slices for IHC staining were incubated at 4°C overnight with the following primary antibodies: SIRT1 (1:100), Mfn2 (1:200), and Drp1 (1:100), after which the corresponding goat anti-rabbit/mouse IgG working solutions (1:1000) were incubated at 37°C for 30 min. The stained slices were observed under the microscope (Olympus Co.) and Image-pro Plus 6.0 software was used to analyze the number of Nissl bodies and protein expression levels in neuronal cells. For immunofluorescence, paraffin slices were fixed, permeabilized and blocked. Then primary antibody against Cyto C (1:200) was performed at 4°C overnight and Alexa Fluor 488 AffiniPure goat anti-rabbit IgG (H + L) was used at room temperature in dark for 30 min. Subsequently, apoptosis in slices was evaluated using the *In Situ* Cell Death Detection Kit (fluorescein). Slices were incubated with fresh TUNEL reaction mixture at 37°C in dark for 1 h. After counterstaining with DAPI, images of the well-prepared slides were performed using a fluorescence microscope (Olympus Co.).

Transmission electric microscopy (TEM)

After fixed using 2.5% pre-cooling glutaraldehyde, hippocampal samples of rats were dissected, post-fixed and prepared according to standard TEM sample preparation protocols [11]. The slices were viewed with one transmission electric microscope (Philips Tecnai 10, Philips Co., Eindhoven, the Netherlands). Mitochondrial area and length were analyzed.

miR-708-3p mimic and inhibitor transfection

The *miR-708-3p* mimic (10 nM), *miR-708-3p* inhibitor (50 nM) and corresponding NC were transfected into cells using Lipofectamine RNAiMax Transfection reagent and Opti-MEMmedium following the manufacturer's instructions.

RT-qPCR

Total RNA was extracted using the TRIzol reagent. Then, SYBR Green PCR Master Mix Reagent Kits were used to quantitate mRNA relative expression with GAPDH as an internal control. All primer sequences are listed in Table S1. For miRNAs, total miRNAs were isolated using the miRcute miRNA Isolation Kit and miRcute Plus miRNA qPCR Kit was used to determine miRNA expression levels with U6 as an internal control. The miRNA primer sequences of *rno-miR-708-3p*, *rno-miR-3085*, *rno-miR-29C-3p*, *rno-miR-194-5p*, and *U6* primers were synthesized from TIANGEN Biotech Co.

(Table S1). Subsequently, RT-qPCR was performed using ABI PRISM 7900 HT PCR system (Applied Biosystems, Thermo Fisher Scientific Inc., Waltham, MA, USA) and relative mRNA or miRNA expression levels were normalized to GAPDH or U6, respectively, using the $2^{-\Delta\Delta CT}$ method.

miRNAs sequencing

According to a previously described protocol, miRNAs sequencing was performed [21]. Briefly, the same total RNA from hippocampal samples was used for small RNA sequencing using an Illumina HiSeq 2500 platform from RiboBio Co. Ltd. (Guangzhou, China). After elimination of low-quality reads of raw data, high-quality reads with length in 18∼26 nucleotide were obtained and aligned with reference genome using miRBase 21.0 by BLAST for identifying known miRNAs and novel −3p and −5p derived miRNAs. Finally, differentially expressed miRNAs were identified by absolute $\log_2$(fold change) ≥ 1 and $P < 0.05$.

miRNAs prediction

Based on the previous study [22], bioinformatics predictions were conducted to identify potential miRNAs targeting SIRT1. The tools miRanda (https://www.mirdb.org/), RNAhybrid (https://directory.fsf.org/wiki/RNAhybrid), and TargetScan (https://www.targetscan.org/) were employed to predict all potential miRNAs which can target SIRT1. Overlapping miRNAs from the three databases were identified and retained for further analyses.

Luciferase reporter assay

On 6-well plates, approximately 1×10^5 HEK-293 T cells expressing miR-708-3p mimic (or mimic NC) per well were co-transfected with vectors with the wild-type or mutant 3′ UTR of *SIRT1*. Lipofectamine 2000 was used as a transfection agent. The ratio of luciferase-to-renilla activities was calculated to normalize for variations in transfection efficiencies according to Dual-Luciferase Reporter Assay System (Promega, Madison, WI, USA).

Statistical analysis

The specific operators in all experiments were blinded to treatment allocations, as were the statistical data analyses. All experiments were performed at least three times, and representative data are shown and presented as mean ± SD. For statistical analysis, SPSS 25.0 statistical software (SPSS Inc., Chicago, IL, USA) was used. Comparison of statistical difference among multiple groups were determined by one-way analysis of variance (ANOVA) followed by Dunnett's test. Significance of difference between two experimental groups was evaluated using independent samples Student's *t* test. A *P* value of < 0.05 was considered statistically significant.

Results

Suppressing SIRT1 with NIC worsens mitochondrial dysfunction and following Cyto C release-driven apoptosis in SH-SY5Y cells under fluoride treatment through disturbing mitochondrial network dynamics

Our recent studies have shown the increase of SIRT1 expression in neuronal cells [20], which suggest that SIRT1 can be a target of fluoride in its neurotoxicity program. To test the potential role of SIRT1 in fluoride neurotoxicity, NIC, a SIRT1 antagonist through exerting feedback inhibitory effects on SIRT1 expression by binding to a conversed pocked near to nicotinamide-adenine dinucleotide [23], was applied to fluoride-treated SH-SY5Y cells. While the protein expression levels of SIRT1 were effectively downregulated (Fig. 1A), NaF-induced lower cellular survival rate was unexpectedly aggravated by NIC (Fig. 1B), with a more robust augment in apoptotic rate (Fig. 1C). Confirming this, the further expression detection of apoptosis-related proteins including cleaved PARP and cleaved caspase-3 were shown dramatically increased by NaF upon co-treatment with NIC (Fig. 1D). Also observed was NaF-induced Cyto C overactivation by the treatment of NIC (Fig. 1E), which was supported by the confocal imaging that large Cyto C puncta were formed, and many of them co-localized with elongated mitochondria (Fig. 1F). Cyto C release from mitochondria and following neuronal cell death always correspond to mitochondrial dysfunction, which is tightly determined by mitochondrial network dynamic processes of fusion and fission [24]. Here, we noticed that SIRT1 inhibition by NIC sensitized cells to NaF-induced mitochondrial dysfunction, manifested as MMP dissipation (Fig. 1G). Further, we observed a more severe state of elongated mitochondria by NaF upon co-treatment with NIC (Fig. 1H). Specifically, the genes that code for mitochondrial fusion/fission dynamics were shown disturbed in response to NaF upon NIC treatment, with facilitated fusion-regulating molecules Mfn1 and Mfn2, along with suppressed fission-regulating molecules Drp1 and Fis1 at protein levels (Fig. 1I). All of these data suggest that NIC exacerbates fluoride-induced mitochondrial dysfunction and Cyto C release-driven apoptosis in SH-SY5Y cells through inhibiting SIRT1 expression and worsening mitochondrial network dynamics.

Overexpressing SIRT1 with Ad-SIRT1 rescues fluoride-induced mitochondrial network dynamics disorder and resultant apoptosis in SH-SY5Y cells

To confirm the role of SIRT1 activation in such neurotoxic process by fluoride, we then generated adenoviruses construct for overexpressing SIRT1 (Ad-SIRT1) that was able to efficiently promote SIRT1 expression levels (Fig. 2A). Of interest, overexpression of SIRT1 reduced the increase in elongated mitochondria upon NaF treatment (Fig. 2B), and this matched well with the changes in the protein levels of decreased fusion and increased fission (Fig. 2C). Additionally, SIRT1 overexpression attenuated NaF-induced reduction of MMP (Fig. 2D). Furthermore, NaF-induced potentiation in Cyto C expression at protein levels was prevented by Ad-SIRT1 (Fig. 2E). Concordantly, in confocal images, formed Cyto C puncta caused by NaF was evidently mitigated with Ad-SIRT1 transfection (Fig. 2F). Meanwhile, we observed concomitant reduction in apoptosis-related proteins including cleaved PARP and cleaved caspase-3 in cells under NaF in combination with Ad-SIRT1 treatment (Fig. 2E). Finally, NaF-induced increase in apoptotic rate and survival rate were rescued in cells transfected with Ad-SIRT1 (Fig. 2G, H). Together, these results show that Ad-SIRT1 recovers the defects in mitochondrial network dynamics and following apoptosis induced by fluoride in SH-SY5Y cells.

SIRT1 mediates fluoride-induced cognitive defects of rats via remodeling mitochondrial network dynamics

We then asked whether the potential function of SIRT1 in pathogenesis of fluoride neurotoxicity exists *in vivo*. To this end, we administered SIRT1 activator RSV or SIRT inhibitor NIC, for 2 months, in rats exposed to NaF (Fig. 3A). As expected, NaF-induced upregulation of SIRT1 levels were further enhanced by RSV and markedly decreased by NIC respectively in both hippocampal and striatal tissues of rats (Fig. 3B), which were also verified by IHC staining (Fig. 3C, Fig. S1A). Further, we observed a significant improved impact on learning and memory impairments of NaF-exposed rats by RSV, as evidenced by the elevated platform crossing numbers (Fig. 3D, E) and more time rats spent in target quadrant (Fig. 3F) in spite of distance rats spent in target quadrant not affected (Fig. 3G). However, when treated with NIC, rat with NaF treatment showed a tendency for worsened learning and memory impairments, although the downregulation of platform crossing numbers, time and distance rats spent in target quadrant did not show statistical significance (Fig. 3D-G). These together revealed the significant involvement of SIRT1 in attenuating the progression of fluoride-induced cognitive defects. Mechanistically,

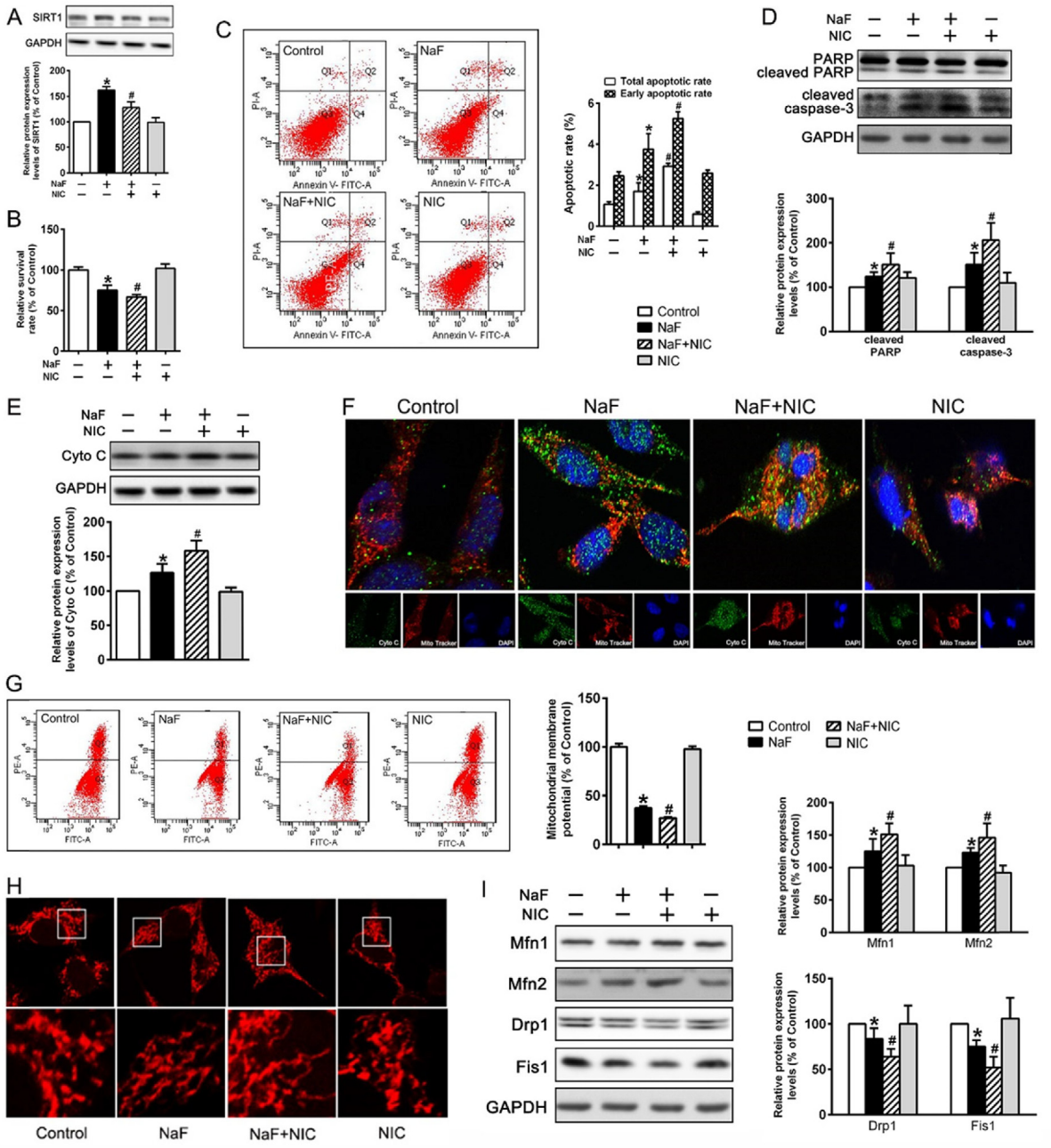

Fig. 1. SIRT1 inhibition by NIC aggravates NaF-induced mitochondrial network dynamics disorder and resultant Cyto C release-driven apoptosis in SH-SY5Y cells. SH-SY5Y cells were cultured with 60 mg/L NaF in the absence or presence of 3 mM NIC for 24 h. (**A**) Representative western blot brands and corresponding density analysis of SIRT1. (**B**) Levels of survival rates in cells detected by CCK-8 assay. (**C**) Representative flow cytometric analysis of apoptotic rates by Annexin V-FITC and PI staining. (**D**) Representative western blot brands and corresponding density analyses of apoptosis-related proteins including cleaved PARP and cleaved caspase-3. (**E**) Representative western blot brands and corresponding density analysis of Cyto C. (**F**) Representative confocal images showing colocalization of Cyto C with mitochondria in cells. Original magnification × 1000. Upper panels were merged views of cells stained for Cyto C (green), MitoTracker CMXRos (red, for mitochondria), and DAPI (blue, for nuclei) in lower panels. (**G**) Representative flow cytometric analysis of MMP by JC-10 staining. (**H**) Representative confocal images showing mitochondrial morphology stained by MitoTracker CMXRos in cells. Original magnification × 1000. Lower panels were magnified views of the areas enclosed by write boxes in upper panels. (**I**) Representative western blot brands and corresponding density analyses of mitochondrial fusion proteins (Mfn1 and Mfn2) and fission proteins (Drp1 and Fis1). GAPDH was used as a loading control for protein expression. Data are represented as mean ± SD from at least three independent experiments. Difference among data were assessed by One-way ANOVA followed by Dunnett's test, * $P < 0.05$ compared with the Control group, # $P < 0.05$ compared with the NaF group. (For interpretation of the references to colour in this figure legend, the reader is referred to the web version of this article.)

treatment of RSV remarkably protected NaF-exposed rats from disordered changes of mitochondrial ultrastructure in neurons as manifested by the reduction in areas and length of mitochondria (Fig. 4A). Correspondingly, NaF-induced imbalance in mitochondrial fusion/fission dynamics was prevented after RSV administration, as the reduction in mitochondrial fusion proteins while the enhancement in mitochondrial fission proteins were noted (Fig. 4B), which was corroborated by the immunoreactivities of Mfn2 and Drp1 in IHC staining in both hippocampal and striatal tissues (Fig. 4C, D, Fig. S1B, C). Additionally, NaF induced an increase in protein expression of Cyto C as well as a decrease in Nissl bodies, and this effected was restrained by RSV (Fig. 4E, F,

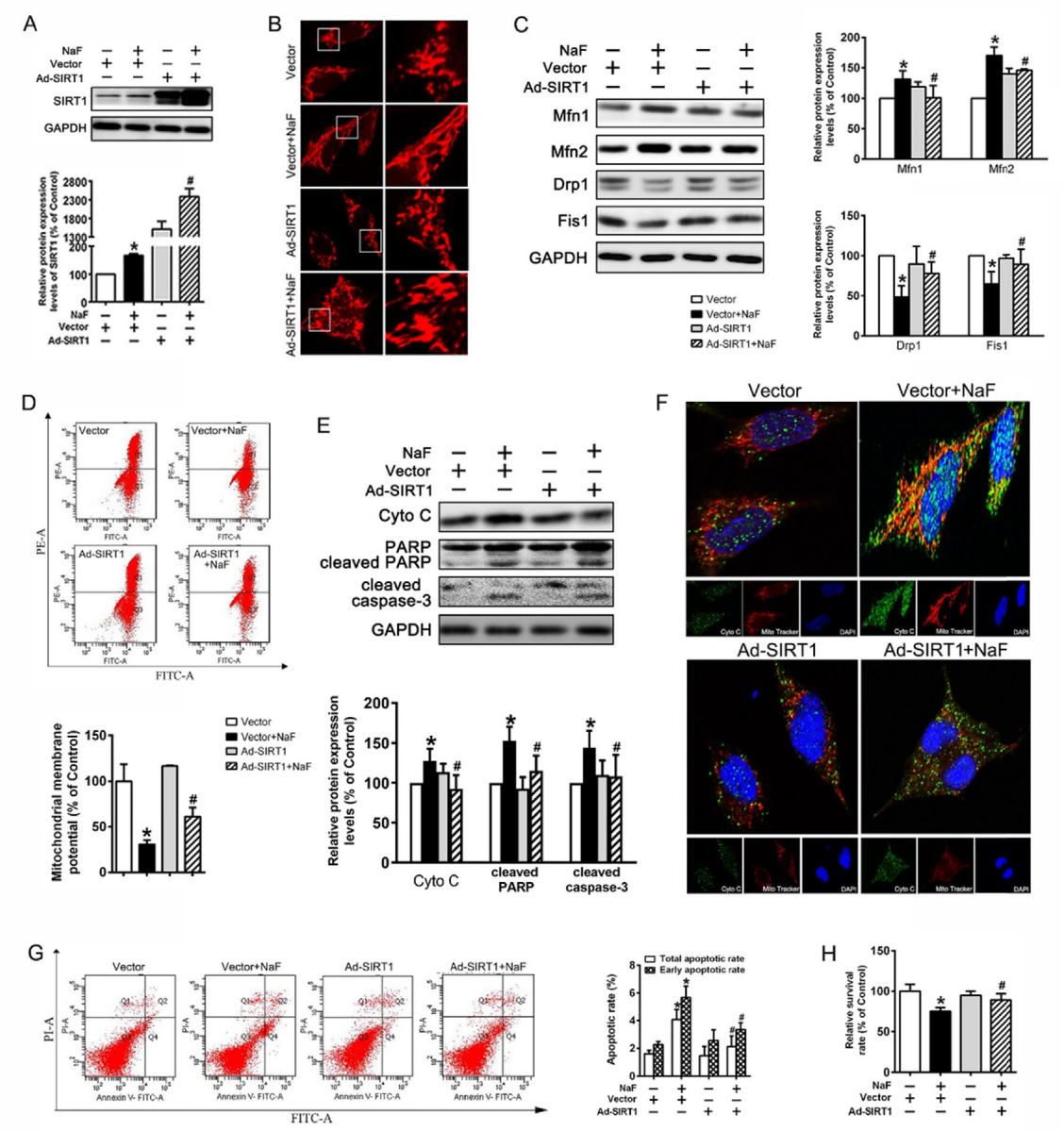

Fig. 2. SIRT1 activation by Ad-SIRT1 alleviates disrupted mitochondrial network dynamics and Cyto C release-driven apoptosis in SH-SY5Y cells treated with NaF. SH-SY5Y cells were cultured with 60 mg/L NaF for 24 h following pretreated infection with adenovirus expressing SIRT1 (Ad-SIRT1, MOI = 200) or control adenovirus (Vector) for 24 h. (**A**) Representative western immunoblots of SIRT1 and corresponding quantitative data were expressed relative to GAPDH. (**B**) Representative confocal images showing mitochondrial morphology stained by MitoTracker CMXRos in cells. Original magnification × 1000. Right panels were the enlarged views of the areas enclosed by write boxes in left panels. (**C**) Representative western immunoblots of mitochondrial fusion proteins (Mfn1 and Mfn2) and fission proteins (Drp1 and Fis1). The corresponding quantitative data were expressed relative to GAPDH. (**D**) Representative flow histograms and quantifications of MMP by JC-10 staining. (**E**) Representative western immunoblots of apoptosis-related proteins including Cyto C, cleaved PARP and cleaved caspase-3, with corresponding quantitative data expressed relative to GAPDH. (**F**) Representative captures of confocal images in cells showing colocalization of Cyto C with mitochondria in cells. Original magnification × 1000. Upper panels were merged views of cells stained for Cyto C (green), MitoTracker CMXRos (red, for mitochondria), and DAPI (blue, for nuclei) in lower panels. (**G**) Representative flow histograms and quantifications of apoptotic rates by Annexin V-FITC and PI staining. (**H**) Levels of survival rates in cells detected by CCK-8 assay. Results are expressed as mean ± SD from at least three independent experiments and were analyzed by one-way ANOVA followed by Dunnett's test. * $P < 0.05$ compared with the Vector group, # $P < 0.05$ compared with the Vector+NaF group. (For interpretation of the references to colour in this figure legend, the reader is referred to the web version of this article.)

Fig. S1D). As again, the accumulation of Cyto C in rising apoptotic neurons with TUNEL staining caused by NaF was rescued upon RSV treatment (Fig. 4G, Fig. S1E). In contract, however, with NIC co-treatment, aforementioned damaged effects of NaF on mitochondrial network dynamics and subsequent eliciting apoptosis in rats' neuronal tissue developed more aggravated (Fig. 4A-G, Fig. S1A-E). Together, these results confirm the significant involvement of SIRT1 in rescuing mitochondrial network dynamics and following apoptosis, thus exerting protective role in the progress of neurobehavioral deficits by fluoride.

SIRT1 is directly targeted by miR-708-3p

We then questioned why SIRT1 is upregulated in response to fluoride. The SIRT1 regulation properties of miRNAs and its therapeutic potential for various human disorders have been intensively studied [14]. Thus, we performed miRNAs transcriptomic profiling and found that among all miRNAs assayed, 42 were significantly upregulated, while 9 were downregulated in hippocampus of fluoride-exposed rats compared with control rats (Fig. 5A, Table S2, 3). Also, we further searched for putative miRNAs of targeting SIRT1 via combining common bioinformatics algorithms of

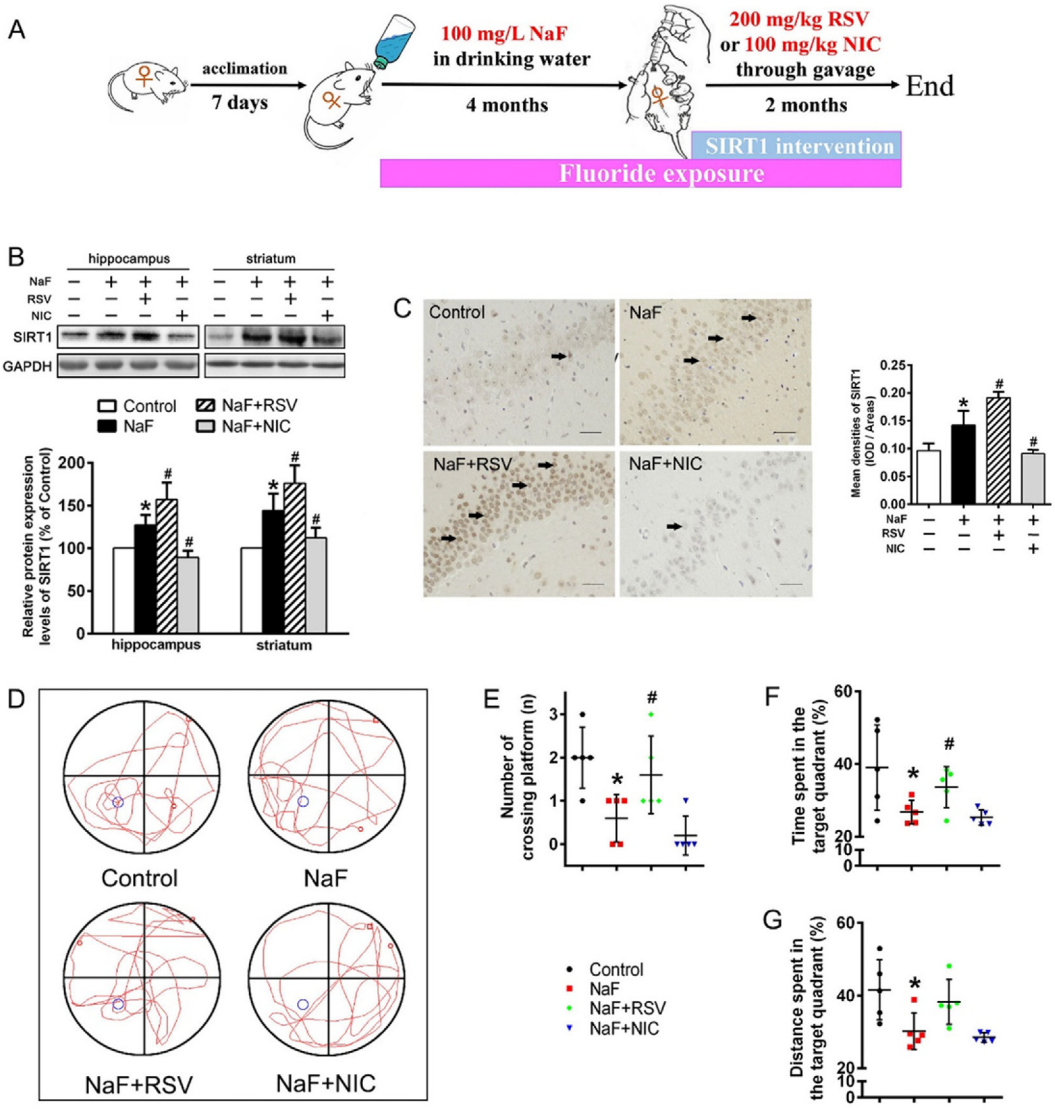

Fig. 3. Learning and memory impairments of rats induced by NaF are alleviated by SIRT1 activation with RSV. SD rats were exposed to 100 mg/L NaF for 6 months, during which rats were treated with 200 mg/kg RSV or 100mk/kg NIC daily through gavage in last 2 months. (**A**) The schematic diagram illustrating the *in vivo* experimental design. (**B**) Representative western blot brands and corresponding density analysis of SIRT1 in hippocampal and striatal tissues (n = 4 rats per group). GAPDH was used as a loading control for protein expression. (**C**) Representative images of IHC staining of SIRT1 in hippocampal CA1 region (scale bar, 50 μm). SIRT1-positive expressed cells are demonstrated by black arrows and quantified (n = 2 rats per group). (**D**) Representative searching traces of rat during the spatial probe test. (**E-G**) The number of crossing platform (**E**), time (**F**) and distance (**G**) rats spent in the target quadrant (%) during the spatial probe test (n = 5 rats per group). Data are represented as mean ± SD. Difference among data were assessed by One-way ANOVA with Dunnett's test, * P < 0.05 compared with the Control group, # P < 0.05 compared with the NaF group.

miRNA prediction programs (miRanda, RNAhybrid, and TargetScan), and a subset of 287 potential miRNAs were obtained (Fig. 5B). Following integrated analysis of above two results, four overlapped miRNAs (*miR-708-3p*, *miR-29c-3p*, *miR-3085*, and *miR-194-5p*) were identified and could regulate SIRT1. Among the selected four miRNAs, only *miR-708-3p* level was confirmed to be substantially downregulated in rat neurons exposed to fluoride (Fig. S2B) and in fluoride-treated SH-SY5Y cells (Fig. S2C). Therefore, we selected *miR-708-3p* for further investigation. To confirm the functional interaction between *miR-708-3p* and SIRT1, we transiently transfected *miR-708-3p* mimic or inhibitor into SH-SY5Y cells. Enforced expression of *miR-708-3p* by mimic was confirmed by qRT-PCR (Fig. 5C), which led to an obvious reduction of SIRT1 mRNA and protein levels (Fig. 5D, E). In contrast, administration of the *miR-708-3p* inhibitor efficiently reduced the expression levels of *miR-708-3p* (Fig. 5F) with concomitant enhanced expression of SIRT1 at gene and protein levels (Fig. 5G, H). In addition, we performed luciferase reporter assay to test whether *miR-708-3p* can influence the expression of SIRT1 by directing targeting SIRT1 3′ UTR (Fig. 5I). SIRT1 3′ UTR WT transfection in HEK293 cells exhibited a lower luciferase activity in the presence of *miR-708-3p* mimic compared with cells transfected SIRT1 3′ UTR WT with *miR-708-3p* NC, while co-transfected SIRT1 3′ UTR MUT with miR-708-3p mimic in HEK293 cells did not show a significant response (Fig. 5J). Collectively, these data validate SIRT1 as a direct target of *miR-708-3p*.

miR-708-3p mediates SIRT1 expression and Cyto C release-driven apoptosis in SH-SY5Y cells under fluoride treatment

Subsequently, we attempted to investigate the influence of *miR-708-3p* on cell susceptibility on fluoride neurotoxicity. Unexpectedly, when *miR-708-3p* expression was enforced using mimic transfection in SH-SY5Y cells, we observed a dramatic deep reduction of cellular survival rate in response to fluoride treatment (Fig. 6A). However, the inhibition of *miR-708-3p* by inhibitor injec-

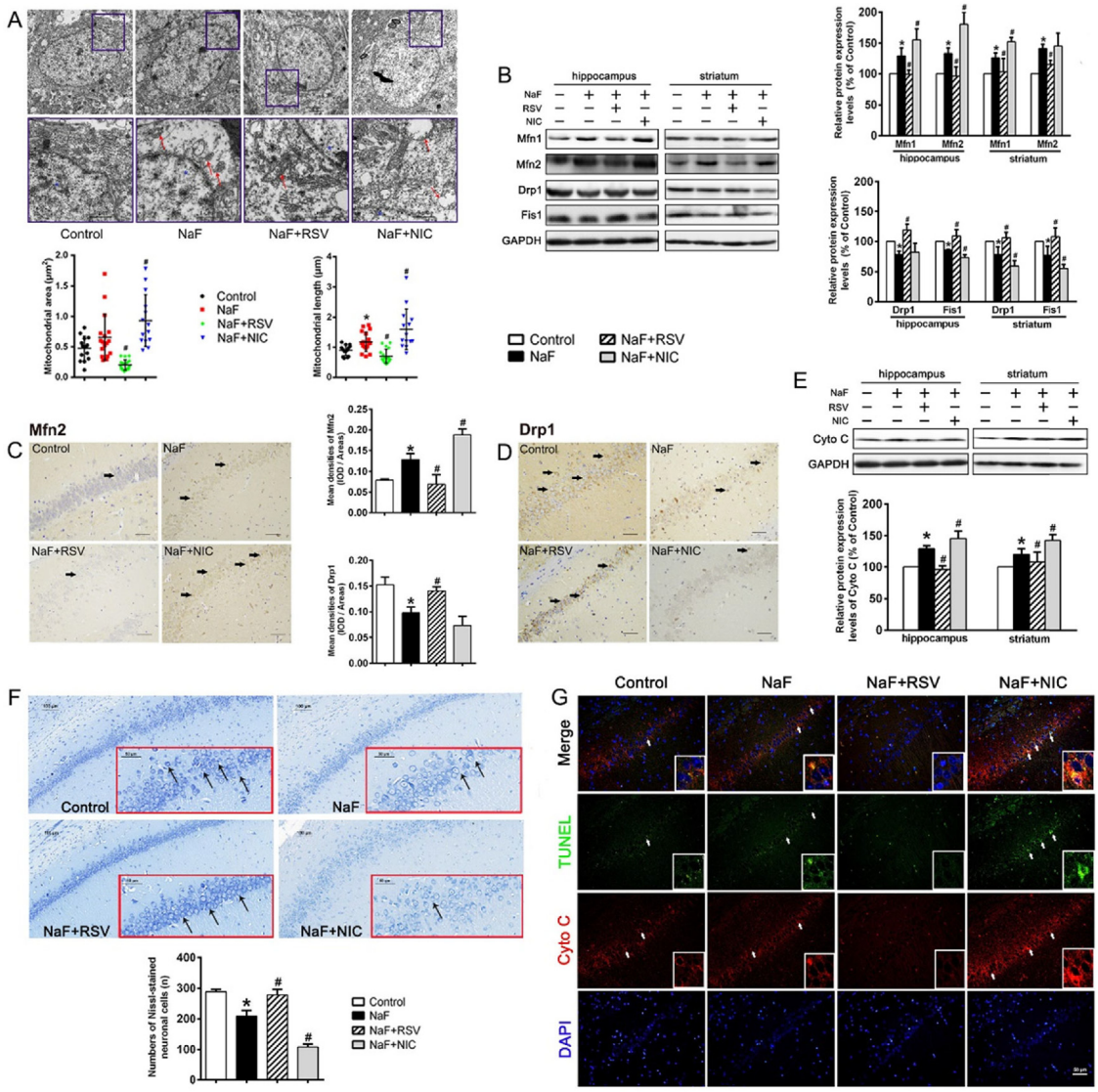

Fig. 4. SIRT1 activation restores, while SIRT1 inhibition further impairs disrupted mitochondrial network dynamics and following Cyto C release-driven apoptosis in neuronal tissues under fluoride treatment. SD rats were exposed to 100 mg/L NaF for 6 months, during which rats were treated with 200 mg/kg RSV or 100mk/kg NIC daily through gavage in last 2 months. (**A**) Representative TEM images of mitochondrial ultrastructure in hippocampal tissues (n = 2 rats per group). The areas indicated by blue boxes in top panel (scale bar, 2 μm) are shown at higher magnification in bottom panel (scale bar, 1 μm). Red arrows, abnormal mitochondrial ultrastructure including swelling and elongation. Asterisk, nuclei. Mitochondrial area and length were quantified. (**B**) Representative western blotting and relative quantifications of mitochondrial fusion and fission proteins in hippocampi and striata (n = 4 rats per group). (**C, D**) Representative images of IHC staining and immunoreactivity quantitative analyses of Mfn2 (**C**) and Drp1 (**D**) in CA1 region of hippocampi (scale bar, 50 μm). Black arrows denote positive expressed cells (n = 2 rats per group). (**E**) Representative western blotting and relative quantifications of Cyto C in hippocampi and striata (n = 4 rats per group). (**F**) Representative captures of Nissl staining in CA1 region of hippocampi (scale bar, 100 μm). Black arrows denote Nissl-positive cells in red boxes (scale bar, 50 μm; n = 2 rats per group). (**G**) Representative images of colocalization of Cyto C expression with TUNEL-labeled neuronal cells in CA1 region of hippocampi (scale bar, 50 μm). TUNEL: green, Cyto C: red, Nuclei: blue with DAPI. Write arrows denote the co-localized cells, typical images of which were shown in write boxes (n = 2 rats per group). Data are represented as mean ± SD. GAPDH was used as a loading control for protein expression. Difference among data were assessed by One-way ANOVA with Dunnett's test, * $P < 0.05$ compared with the Control group, # $P < 0.05$ compared with the NaF group. (For interpretation of the references to colour in this figure legend, the reader is referred to the web version of this article.)

tion led to an obvious reactivation of cell survival rate (Fig. 6A). Furthermore, we observed that the fluoride-treated cells transfected with *miR-708-3p* mimic showed markedly repressed protein expression of SIRT1 (Fig. 6B) and led to the aggravation of fluoride-induced apoptosis-related proteins, as shown by increased protein expression of cleaved PARP and cleaved caspase-3 (Fig. 6C). In contrast, *miR-708-3p* inhibitor was able to effectively inhibit fluoride-induced apoptosis (Fig. 6E) associated with SIRT1 overactivation (Fig. 6D). Moreover, overexpression of *miR-708-3p* sensitized fluoride to exaggerate the protein expression of Cyto C (Fig. 6F), while downregulation of *miR-708-3p* showed a strong inhibitory effect on Cyto C activation in the presence of fluoride (Fig. 6G). Concomitantly, the formed Cyto C puncta in cells with fluoride treatment was also markedly increased by *miR-708-3p* mimic but reduced after introducing *miR-708-3p* inhibitor (Fig. 6H). These results demonstrate that *miR-708-3p* mediates fluoride-induced changes of SIRT1 expression and Cyto C release-driven apoptosis in SH-SY5Y cells.

miR-708-3p mediates fluoride-induced mitochondrial network dynamics disorders and resulting Cyto C release-apoptosis by directly targeting SIRT1

The regulation of *miR-708-3p* on SIRT1 expression led us to confirm whether the physiological significance of *miR-708-3p* in fluoride neurotoxicity is indeed through SIRT1-dependent pathway.

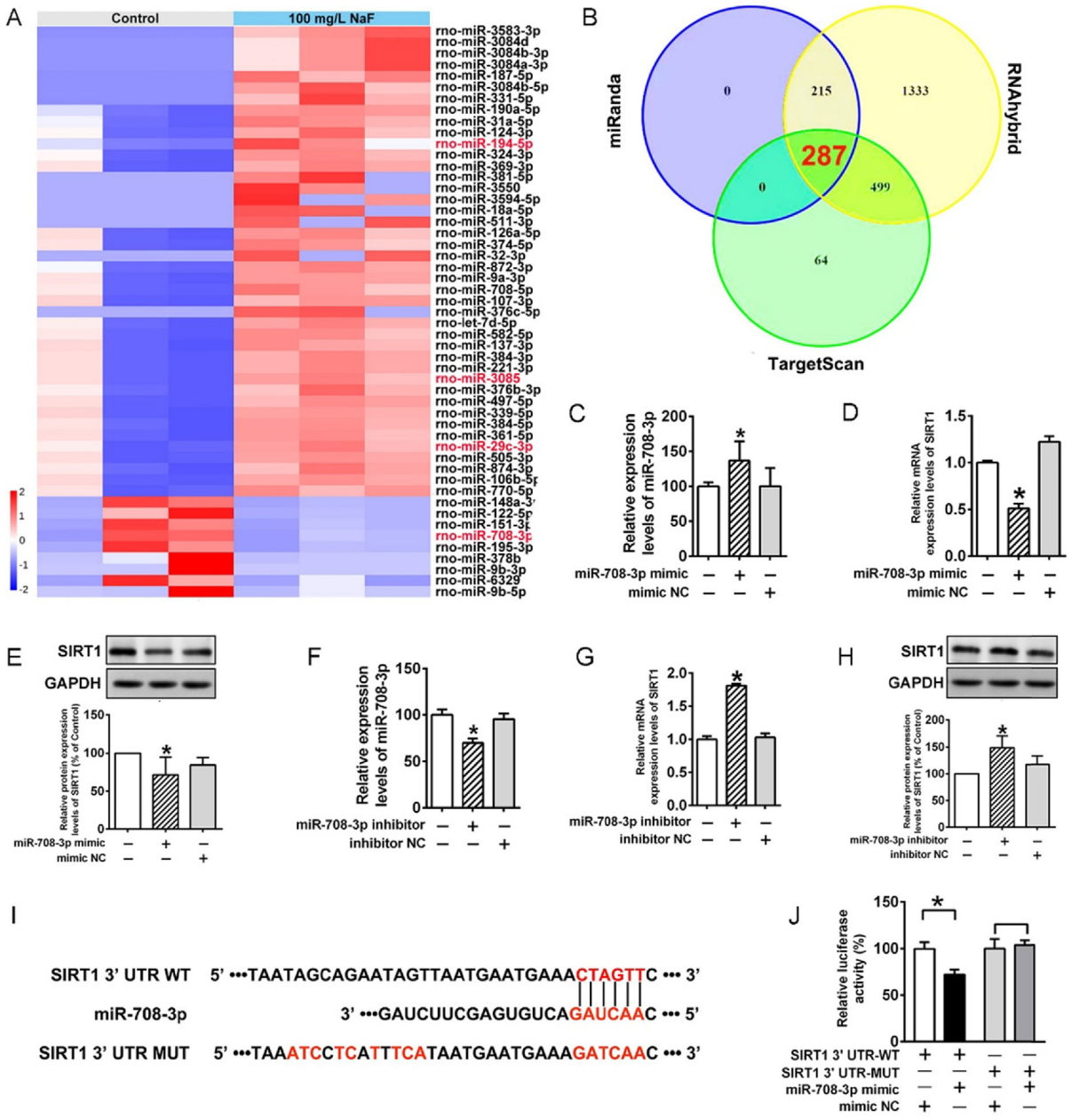

Fig. 5. SIRT1 is targeted by *miR-708-3p* directly. (**A**) Heatmap depicting differentially expressed miRNAs (adjusted *P* value < 0.05 and absolute $\log_2$(fold change) ≥ 1) in rats exposed to 100 mg/L NaF compared with the Control rats (n = 3 rats each group). The selected four miRNAs candidates were noted in red. (**B**) Venn diagram showing the overlap of predicted 287 potential miRNAs of targeting SIRT1 using miRNA databases including miRanda, RNAhybrid, and TargetScan. (**C-E**) Relative changes of *miR-708-3p* expression (**C**), mRNA (**D**) and protein (**E**) levels of SIRT1 in SH-SY5Y cells following transfection with *miR-708-3p* mimic. (**F-H**) *miR-708-3p* expression (**F**), mRNA (**G**) and protein (**H**) levels of SIRT1 in SH-SY5Y cells following transfection with *miR-708-3p* inhibitor. miRNA levels are expressed as a ratio to *U6*; mRNA levels are expressed as a ratio to *GAPDH*. (**I**) Sequence of *miR-708-3p* potential binding sites within the 3′ UTR of SIRT1 mRNA showing in red and the site-directed construction of SIRT1 3′UTR mutants (MUT). (**J**) Luciferase activities detected in HEK293T cells showing the effect of *miR-708-3p* mimic transfection on activity of the reporter containing SIRT1 3′UTR with a putative miR-708-3p recognition element. Data are represented as mean ± SD from at least three independent experiments. Difference among data were assessed by One-way ANOVA with Dunnett's test. For C–H, * $P < 0.05$ compared with the Control group. For J, * $P < 0.05$ compared with the SIRT1 3′UTR-WT + mimic NC group. (For interpretation of the references to colour in this figure legend, the reader is referred to the web version of this article.)

Overactivation of SIRT1 in cells with Ad-SIRT1 transfection (Fig. 7A) effectively rescued the deleterious effect of *miR-708-3p* mimic in disordered mitochondrial network dynamics caused by fluoride, as evidenced by the reduction of fusion proteins along with the increase of fission proteins, and the improved mitochondrial morphology (Fig. 7B, C). As well, fluoride-triggered increase in Cyto C and cleaved caspase-3 protein levels accompanied with the accumulation of Cyto C puncta co-localized with mitochondria were worsened by *miR-708-3p* mimic, which were restored upon co-treatment with Ad-SIRT1 (Fig. 7D, E). On the other hand, after treatment with NIC, to further inhibit SIRT1 activation in *miR-708-3p* down-expressing cells with fluoride treatment (Fig. 7F), shifts in mitochondrial fusion/fission dynamics proteins were conferred toward increased fusion and decreased fission (Fig. 7G), a result consistent with the phenomenon with more lengthened structural architecture of mitochondria (Fig. 7H). Furthermore, the beneficial effect of *miR-708-3p* inhibition in fluoride-induced apoptosis were counteracted in the presence of NIC, as shown by the aggravation of Cyto C puncta co-localized with mitochondria as well as the increased protein levels of Cyto C and cleaved

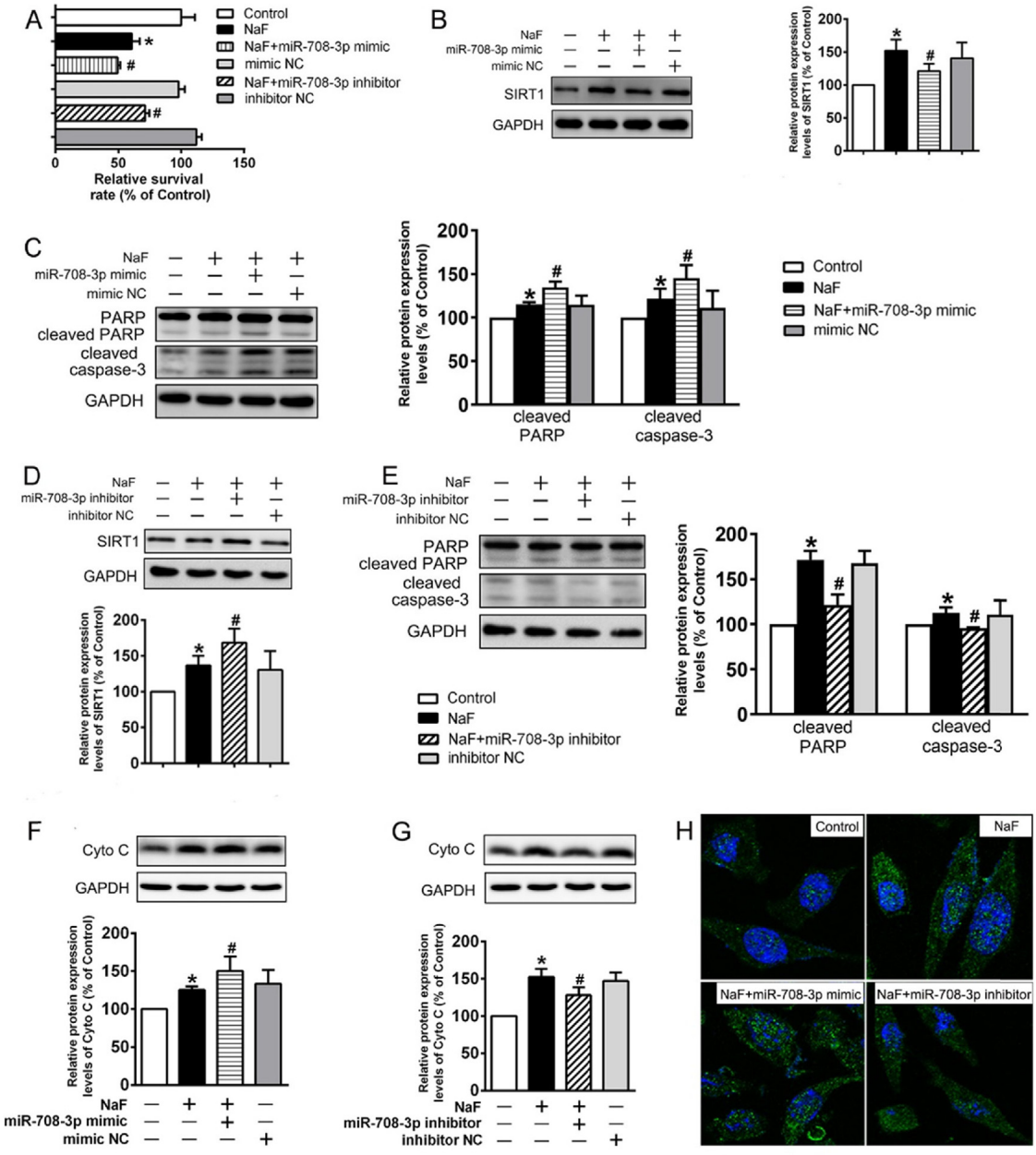

Fig. 6. *miR-708-3p* regulates fluoride-induced changes of SIRT1 expression and Cyto C release-driven apoptosis in SH-SY5Y cells. SH-SY5Y cells were cultured with 60 mg/L NaF for 24 h after infection of 10 nM *miR-708-3p* mimic (or 50 nM *miR-708-3p* inhibitor) or corresponding NC for 24 h. (**A**) Levels of cellular survival rats detected by CCK-8 assay. (**B-C**) Representative western blot brands and corresponding density analyses of SIRT1 (**B**) and apoptosis-related proteins (cleaved PARP and cleaved caspase-3) (**C**) in cells co-cultured with NaF and *miR-708-3p* mimic. (**D-E**) Representative western blot brands and corresponding density analyses of SIRT1 (**D**) and apoptosis-related proteins (cleaved PARP and cleaved caspase-3) (**E**) in cells co-cultured with NaF and *miR-708-3p* inhibitor. (**F**) Representative western blot brands and corresponding density analyses of Cyto C in cells co-cultured with NaF and *miR-708-3p* mimic. (**G**) Representative western blot brands and corresponding density analyses of Cyto C in cells co-cultured with NaF and miR-708-3p inhibitor. (**H**) Representative confocal images of Cyto C-labeled (green) cells, nuclei were stained with DAPI (blue). Original magnification × 1000. GAPDH was used as a loading control for protein expression. Data are represented as mean ± SD from at least three independent experiments. Difference among data were assessed by One-way ANOVA followed by Dunnett's test, * $P < 0.05$ compared with the Control group, # $P < 0.05$ compared with the NaF group. (For interpretation of the references to colour in this figure legend, the reader is referred to the web version of this article.)

caspase-3 (Fig. 7I, J). These results strongly suggest that *miR-708-3p* regulates mitochondrial network dynamics disruption and following apoptosis in fluoride-treated cells through directly targeting SIRT1.

Discussion

SIRT1 is widely expressed in neurons and the downregulation of SIRT1 expression grows the increased risk for developmental of brain diseases [25]. In brain tissues of patients suffering from Alzheimer's disease, the expression of SIRT1 was decreased [26]. However, with regard to fluoride-induced neurotoxicity, data from our present and previous study both showed that fluoride-exposed rats displayed cognitive impairments along with enhanced SIRT1 expression [20]. Similarly, induction of SIRT1 levels were also observed in different tissues under fluoride treatment including ameloblast-derived LS8 cells [27] and serum of female rats and women [28,29], which are considered as an insufficient adaptive protective response. To confirm our results, we further demon-

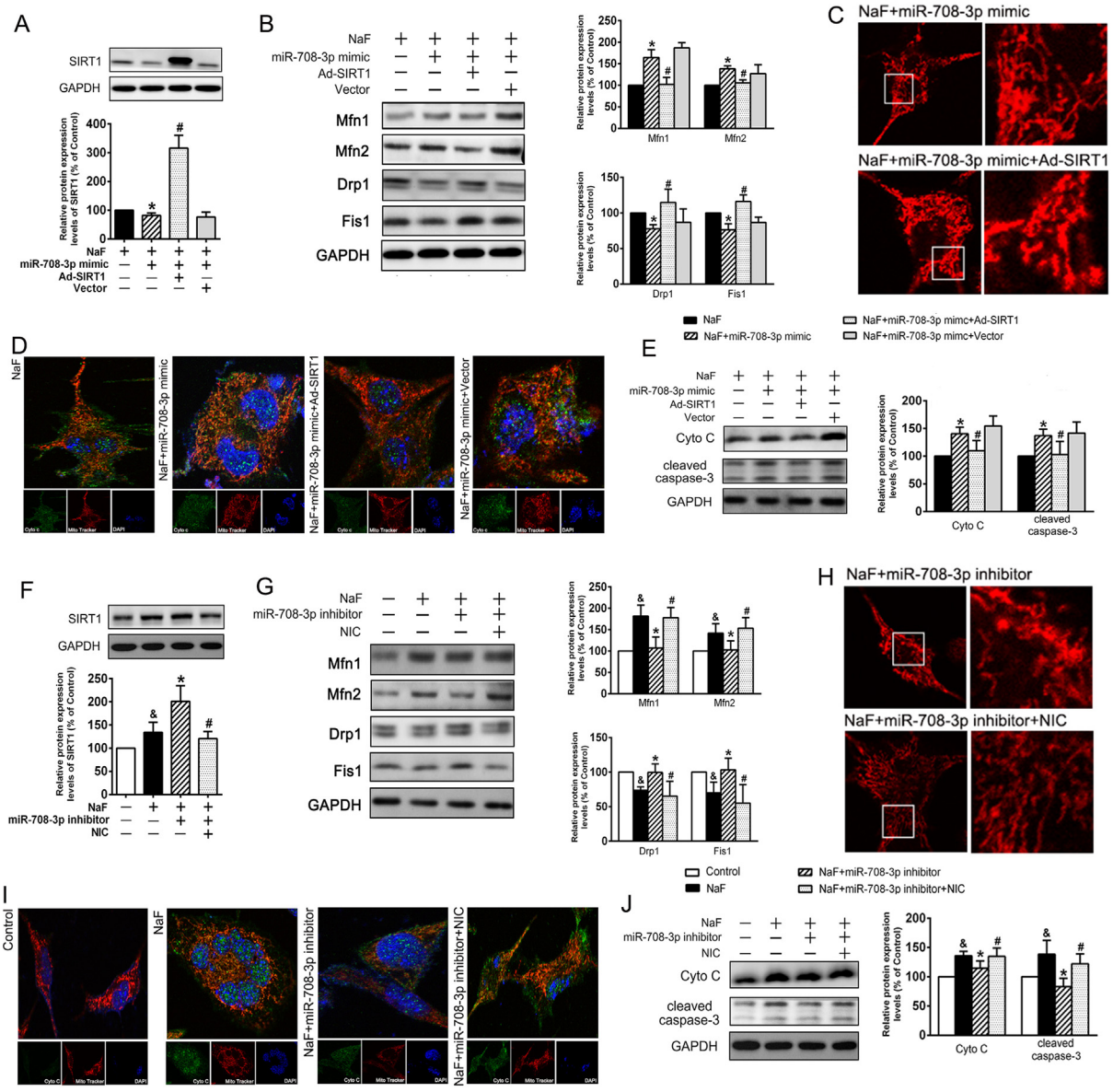

Fig. 7. ***miR-708-3p*** **regulates disrupted mitochondrial network dynamics and resulting Cyto C release-driven apoptosis in NaF-treated SH-SY5Y cells by directly targeting SIRT1.** For **A-E**, after infection with *miR-708-3p* mimic (10 nM) plus Ad-SIRT1 (MOI = 200) or Vector for 24 h, SH-SY5Y cells were cultured with 60 mg/L NaF for 24 h. (**A**) Representative western immunoblots of SIRT1 and corresponding quantitative data were expressed relative to GAPDH. (**B**) Representative western immunoblots of mitochondrial fusion and fission proteins, with density analyses expressed relative to GAPDH. (**C**) Representative confocal images showing mitochondrial morphology stained by MitoTracker CMXRos in cells. Original magnification × 1000. Right panels were the enlarged views of the areas enclosed by write boxes in left panels. (**D**) Representative confocal images showing colocalization of Cyto C with mitochondria in cells. Original magnification × 1000. Upper panels were merged views of cells stained for Cyto C (green), MitoTracker CMXRos (red, for mitochondria), and DAPI (blue, for nuclei) in lower panels. (**E**) Representative western immunoblots of apoptosis-related proteins including Cyto C and cleaved caspase-3, with density analyses expressed relative to GAPDH. For **F-J**, after infection with *miR-708-3p* inhibitor (50 nM) for 24 h, SH-SY5Y cells were cultured with 60 mg/L NaF in the absence or presence of 3 mM NIC for 24 h. (**F**) Representative western immunoblots of SIRT1 and corresponding quantitative data were expressed relative to GAPDH. (**G**) Representative western immunoblots of mitochondrial fusion and fission proteins, with density analyses expressed relative to GAPDH. (**H**) Representative confocal images showing mitochondrial morphology stained by MitoTracker CMXRos in cells. Original magnification × 1000. Right panels were the enlarged views of the areas enclosed by write boxes in left panels. (**I**) Representative confocal images showing colocalization of Cyto C with mitochondria in cells. Original magnification × 1000. Upper panels were merged views of cells stained for Cyto C (green), MitoTracker CMXRos (red, for mitochondria), and DAPI (blue, for nuclei) in lower panels. (**J**) Representative western immunoblots of apoptosis-related proteins including Cyto C and cleaved caspase-3, with density analyses expressed relative to GAPDH. Data are represented as mean ± SD from at least three independent experiments. Difference among data were assessed by One-way ANOVA followed by Dunnett's test, $^{\&}$ $P < 0.05$ compared with the Control group, * $P < 0.05$ compared with the NaF group, $^{\#}$ $P < 0.05$ compared with the NaF + *miR-708-3p* mimic (or inhibitor) group. (For interpretation of the references to colour in this figure legend, the reader is referred to the web version of this article.)

strated that learning and memory impairments of fluoride-exposed rats were effectively attenuated after promotion of SIRT1 by RSV but were worsened after suppression of SIRT1 by NIC, suggesting the important protective involvement of SIRT1 activation against cognitive defects induced by fluoride.

The therapeutic significance of SIRT1 in diverse neurological disorders via it-mediated signaling pathways has been well accepted and established [30]. Till it has been well reported about the regulation of SIRT1 on target molecules involved in apoptosis [31]. In a study investigating the influence of folic acid on

fluoride-treated oocytes, folic acid were proven exerting a beneficial effect by impeding apoptosis via a SIRT1 dependent mechanism [32]. Our previous study showed that fluoride caused apoptosis by inhibiting SIRT1 activation in SH-SY5Y cells [10]. Here, combining *in vivo* and *in vitro* models, we further validated that fluoride-induced apoptosis detected by the increase of cleaved PARP and cleaved caspase-3 levels were suppressed by activating SIRT1 and in turn aggravated after inhibiting SIRT1. Consistently, the protective effect of dihydronicotinamide riboside-induced hair-cell were antagonized by inhibition of SIRT1 and alleviated by activation of SIRT1 [33]. In particular, Cyto C release from mitochondria reduced by fluoride were rescued by SIRT1 activation whereas exacerbated by SIRT1 inhibition, were further demonstrated in our current study. This is in consistence with recent work showing the protective role of SRIT1 in conveying fluoride-caused apoptosis in osteoblast-like MC3T3-E1 cells [34] and in ameloblast-derived LS8 cells [27]. Herein, all of these data provided compelling evidence showing the crucial role of SIRT1-alleviated Cyto C-driven apoptosis pathway in neurotoxic process from fluoride injuries.

Cyto C activation, the critical event in apoptosis, releases from mitochondria and often reflects dysfunction of mitochondria [35]. There is growing evidence indicating that SIRT1 is a promising molecular target for the treatment of mitochondrial dysfunction and neurological disorders via regulating mitochondrial quality control [36,37]. Notably, homeostasis of mitochondrial network dynamics is crucial for maintaining normal mitochondrial function [38]. In our previous study, mitochondrial fusion/fission disequilibrium characterized by fusion promotion/fission suppression was found contributing to fluoride neurotoxicity [11]. Our results further confirmed that SIRT1 inhibition exacerbated, while SIRT1 activation recovered the imbalance of mitochondrial fusion/fission phenotypes as well as resulting over-elongated structure and dysfunction of mitochondria induced by fluoride, suggestive of the connections between SIRT1 and mitochondrial network dynamics, namely SIRT1 activation exerted neuroprotective actions under fluoride treatment via restoring mitochondrial network dynamics. Our results are concordant with the findings in a prior study concerning the cardioprotection of SIRT1 against ischemia/reperfusion (I/R) injury, where age-related deficiency of SIRT1 contributed to the higher alterations of Mfn1 and Mfn2, resulting in cardiac dysfunction by I/R [39]. However, there has been some controversy regarding the function of SIRT1 in mitochondrial fusion/fission dynamics. For example, in studies exploring the therapeutic intervention against hypoxia/reoxygenation-induced cardiac dysfunction, RSV promoted both mitochondrial fission and fusion to regulate mitochondrial mass [40]. Another study on mitochondrial network fragmentation in cadmium (Cd)-treated hepatic cells, the alleviation of Cd-induced mitochondrial ultrastructural damage by puerarin, manifested by inhibited fusion protein levels and enhanced fission protein levels, were markedly reversed by SIRT1 knockdown [41]. Although mitochondrial network dynamics exhibited differently in various studies, mitochondria undergo disruption of mitochondrial network integrity once the balance of fusion and fission were broken [42]. Given the possible difference in susceptibility of mitochondrial network dynamics under different environment of toxicant exposure, our results highlighted the alleviative effects of SIRT1 in fluoride-induced neuronal damage via reshaping mitochondrial network dynamics.

Nowadays SIRT1 has been reported to be negatively regulated by several miRNAs in various biological mechanisms of diseases [43]. Accordingly, we hypothesized that SIRT1 may constitute an important target regulated by miRNAs in fluoride neurotoxicity, as deregulated miRNAs have been reported in not only human osteoblasts [44] but also hippocampus [19] in *in vivo* fluoride models. Additionally, elevated *miR-221-3p* was observed in fluoride-treated PC12 cells in our prior study [45]. In this regard, miRNAs targeting SIRT1 were firstly screened based on the results of miRNAs sequencing and bioinformatic analyses, with stable downregulated *miR-708-3p* in *in vivo* and *in vitro* fluoride models selected ultimately. Here, we further observed that *miR-708-3p* mimic suppressed, while *miR-708-3p* inhibitor promoted SIRT1 expression, which further confirmed the targeting relationship between *miR-708-3p* and SIRT1. Also, miRNAs are known to be able to bind to 3′ UTR of mRNA and inhibit mRNA protein translation [46]. Luciferase reporter assay in this work verified the direct link between *miR-708-3p* and its binding site within SIRT1 mRNA. These findings are the first, to our knowledge, to report SIRT1 as a direct target gene of *miR-708-3p*.

Only a few studies focusing on dysregulated *miR-708-3p* expression were documented in recently years. In the lung of post-COVID-19 patients, expression of *miR-708-3p* presented a downregulation [47]. Moreover, *miR-708-3p* was found to be decreased and overexpression of *miR-708-3p* alleviate progression of diseases including myocardial infarction [48], breast cancer [49], and idiopathic pulmonary fibrosis [50]. In this work, despite *miR-708-3p* downregulation in SH-SY5Y cells under fluoride treatment, however, we observed that mitochondrial abnormalities along with following apoptosis induced by fluoride were counteracted by *miR-708-3p* inhibitor and in turn worsened by *miR-708-3p* mimic, suggesting the restorative effects of *miR-708-3p* decrease in fluoride-caused cell death. In common with our results, in both the bone tissue of postmenopausal osteoporosis rat model and osteoporosis patients, *miR-708-3p* was highly expressed and positively regulated osteoclast differentiation [51]. This is the first study reporting the potential role of *miR-708-3p* inhibition in alleviating development of neuronal death by fluoride. In this paper, besides, we systematically and rigorously investigated the regulatory mechanisms of *miR-708-3p* in fluoride neurotoxicity and strongly indicated that the protective roles of *miR-708-3p* inhibition in fluoride-induced neuronal injury was indeed through stimulating SIRT1 expression directly and following restoration of mitochondrial network dynamics *in vitro*. Alike, in late-stage Parkinson's disease, upregulation of *miR-543* triggered SIRT1 inhibition and influenced the early white matter alterations observed in patients [52]. Still, future studies are required to verify with statistical confidence the biological function of *miR-708-3p* in *in vivo* model of fluoride neurotoxicity.

Our study still has some limitations. First, it is noteworthy that among sirtuin family members, SIRT1 and SIRT3, localized to the nucleus and mitochondria respectively, is both critical in maintaining mitochondrial homeostasis and the potential roles of their interaction have been explored [53,54]. Considering that neuronal injury induced by fluoride is partly mediated by SIRT3 inhibition reported in a previous study [55], it is necessary to carry out further investigation aiming at determining whether fluoride-induced abnormal mitochondrial network dynamics is regulated directly by SIRT1 or through the interaction of SIRT1 with SIRT3. Another limitation is that we mainly focused on alterations in SH-SY5Y cells and female rats in the current study. More exhibition of data in male rats and primary neuronal cells are still needed in the following studies to confirm our findings comprehensively.

Conclusions

In summary, the *in vitro* and *in vivo* bidirectional targeting regulations of SIRT1 were used to validate that SIRT1 activation exerted a protective role in neuronal injuries induced by fluoride via restoring mitochondrial network dynamics disorders and following Cyto C release-driven apoptosis. More importantly, we revealed an unreported role of *miR-708-3p* as identified targeting

SIRT1 under fluoride-injured conditions. Altogether, these results underscore the functional importance of SIRT1 activation in neurotoxic process of fluoride and further hint at the beneficial effects of inhibiting *miR-708-3p*, an upstream regulator of targeting SIRT1. Our findings may help to establish new theoretical basis for improving preventative and therapeutic options for neurotoxic progression by fluoride.

Ethics requirements

All rat experiments were carried out in accordance with the Guidelines for the Care and Use of Laboratory Animals published by Ministry of Health People's Republic of China and approved by the Ethics Review Committee for Animal Research at Huazhong University of Science and Technology (Approval No. HUST NY/MA-029-2018).

CRediT authorship contribution statement

Qian Zhao: Investigation, Writing – original draft. **Guo-yu Zhou:** Investigation, Methodology. **Qiang Niu:** Data curation, Investigation. **Jing-wen Chen:** . **Pei Li:** Methodology, Validation. **Zhi-yuan Tian:** . **Dong-jie Li:** Visualization, Formal analysis. **Tao Xia:** Methodology, Validation. **Shun Zhang:** Supervision, Writing – review & editing. **Ai-guo Wang:** Conceptualization, Supervision, Funding acquisition, Writing – review & editing.

Declaration of competing interest

The authors declare that they have no known competing financial interests or personal relationships that could have appeared to influence the work reported in this paper.

Acknowledgements

This work was supported by grants from the National Natural Science Foundation of China (Grants No. 82073515, and No. 81773388), the State Key Program of National Natural Science of China (Grant No. 81430076).

Appendix A. Supplementary material

Supplementary data to this article can be found online at https://doi.org/10.1016/j.jare.2023.11.032.

References

[1] More L, Lauterborn JC, Papaleo F, Brambilla R. Enhancing cognition through pharmacological and environmental interventions: Examples from preclinical models of neurodevelopmental disorders. Neurosci Biobehav Rev 2020;110:28–45. doi: https://doi.org/10.1016/j.neubiorev.2019.02.003.

[2] Vellingiri B, Suriyanarayanan A, Selvaraj P, Abraham KS, Pasha MY, Winster H, et al. Role of heavy metals (copper (Cu), arsenic (As), cadmium (Cd), iron (Fe) and lithium (Li)) induced neurotoxicity. Chemosphere 2022; 301:134625. doi:10.1016/j.chemosphere.2022.134625.

[3] Peckham S, Awofeso N. Water fluoridation: a critical review of the physiological effects of ingested fluoride as a public health intervention. ScientificWorldJournal 2014;2014:293019. doi: https://doi.org/10.1155/2014/293019.

[4] Balasubramanian S, Perumal E. A systematic review on fluoride-induced epigenetic toxicity in mammals. Crit Rev Toxicol 2022:1–20. doi: https://doi.org/10.1080/10408444.2022.2122771.

[5] Nadei OV, Khvorova IA, Agalakova NI. Cognitive decline of rats with chronic fluorosis is associated with alterations in hippocampal calpain signaling. Biol Trace Elem Res 2020;197:495–506. doi: https://doi.org/10.1007/s12011-019-01993-z.

[6] Chen J, Niu Q, Xia T, Zhou G, Li P, Zhao Q, et al. ERK1/2-mediated disruption of BDNF-TrkB signaling causes synaptic impairment contributing to fluoride-induced developmental neurotoxicity. Toxicology 2018;410:222–30. doi: https://doi.org/10.1016/j.tox.2018.08.009.

[7] Ren C, Zhang P, Yao XY, Li HH, Chen R, Zhang CY, et al. The cognitive impairment and risk factors of the older people living in high fluorosis areas: DKK1 need attention. BMC Public Health 2021;21:2237. doi: https://doi.org/10.1186/s12889-021-12310-6.

[8] Li X, Feng Y, Wang XX, Truong D, Wu YC. The critical role of SIRT1 in Parkinson's disease: Mechanism and therapeutic considerations. Aging Dis 2020;11:1608–22. doi: https://doi.org/10.14336/AD.2020.0216.

[9] Ye F, Wu A. The protective mechanism of SIRT1 in the regulation of mitochondrial biogenesis and mitochondrial autophagy in Alzheimer's disease. J Alzheimers Dis 2021;82:149–57. doi: https://doi.org/10.3233/JAD-210132.

[10] Tu W, Zhang Q, Liu Y, Han L, Wang Q, Chen P, et al. Fluoride induces apoptosis via inhibiting SIRT1 activity to activate mitochondrial p53 pathway in human neuroblastoma SH-SY5Y cells. Toxicol Appl Pharmacol 2018;347:60–9. doi: https://doi.org/10.1016/j.taap.2018.03.030.

[11] Zhao Q, Niu Q, Chen J, Xia T, Zhou G, Li P, et al. Roles of mitochondrial fission inhibition in developmental fluoride neurotoxicity: mechanisms of action in vitro and associations with cognition in rats and children. Arch Toxicol 2019;93:709–26. doi: https://doi.org/10.1007/s00204-019-02390-0.

[12] Rasmussen ML, Gama V. A connection in life and death: The BCL-2 family coordinates mitochondrial network dynamics and stem cell fate. Int Rev Cell Mol Biol 2020;353:255–84. doi: https://doi.org/10.1016/bs.ircmb.2019.12.005.

[13] Santovito D, Weber C. Non-canonical features of microRNAs: paradigms emerging from cardiovascular disease. Nat Rev Cardiol 2022;19:620–38. doi: https://doi.org/10.1038/s41569-022-00680-2.

[14] Zia A, Sahebdel F, Farkhondeh T, Ashrafizadeh M, Zarrabi A, Hushmandi K, et al. A review study on the modulation of SIRT1 expression by miRNAs in aging and age-associated diseases. Int J Biol Macromol 2021;188:52–61. doi: https://doi.org/10.1016/j.ijbiomac.2021.08.013.

[15] Raucci A, Macri F, Castiglione S, Badi I, Vinci MC, Zuccolo E. MicroRNA-34a: the bad guy in age-related vascular diseases. Cell Mol Life Sci 2021;78:7355–78. doi: https://doi.org/10.1007/s00018-021-03979-4.

[16] Mingardi J, La Via L, Tornese P, Carini G, Trontti K, Seguini M, et al. miR-9-5p is involved in the rescue of stress-dependent dendritic shortening of hippocampal pyramidal neurons induced by acute antidepressant treatment with ketamine. Neurobiol Stress 2021;15:100381. doi: https://doi.org/10.1016/j.ynstr.2021.100381.

[17] Zhao Y, Yu Y, Ommati MM, Xu J, Wang J, Zhang J, et al. Multiomics analysis revealed the molecular mechanism of miRNAs in fluoride-induced hepatic glucose and lipid metabolism disorders. J Agric Food Chem 2022;70:14284–95. doi: https://doi.org/10.1021/acs.jafc.2c03049.

[18] Luo Y, Da D, Weng Q, Yao S, Zhang H, Han X, et al. miR-296-5p promotes autophagy in mouse LS8 cells under excessive fluoride via AMPK/ULK1 pathways. Ecotoxicol Environ Saf 2022;235:113362. doi: https://doi.org/10.1016/j.ecoenv.2022.113362.

[19] Wang J, Zhang Y, Guo Z, Li R, Xue X, Sun Z, et al. Effects of perinatal fluoride exposure on the expressions of miR-124 and miR-132 in hippocampus of mouse pups. Chemosphere 2018;197:117–22. doi: https://doi.org/10.1016/j.chemosphere.2018.01.029.

[20] Zhao Q, Tian Z, Zhou G, Niu Q, Chen J, Li P, et al. SIRT1-dependent mitochondrial biogenesis supports therapeutic effects of resveratrol against neurodevelopment damage by fluoride. Theranostics 2020;10:4822–38. doi: https://doi.org/10.7150/thno.42387.

[21] Pritchard CC, Cheng HH, Tewari M. MicroRNA profiling: approaches and considerations. Nat Rev Genet 2012;13:358–69. doi: https://doi.org/10.1038/nrg3198.

[22] Chen Z, Ou D, Huang Z, Shen P. Identification of hsa_circ_0002024 as a prognostic competing endogenous RNA (ceRNA) through the hsa_miR_129-5p/Anti-Silencing Function 1B Histone Chaperone (ASF1B) axis in renal cell carcinoma. Bioengineered 2021;12:6579–93. doi: https://doi.org/10.1080/21655979.2021.1974650.

[23] Nikas IP, Paschou SA, Ryu HS. The role of nicotinamide in cancer chemoprevention and therapy. Biomolecules 2020:10. doi: https://doi.org/10.3390/biom10030477.

[24] Sabouny R, Shutt TE. Reciprocal regulation of mitochondrial fission and fusion. Trends Biochem Sci 2020;45:564–77. doi: https://doi.org/10.1016/j.tibs.2020.03.009.

[25] Batiha GE, Al-Kuraishy HM, Al-Gareeb AI, Elekhnawy E. SIRT1 pathway in Parkinson's disease: a faraway snapshot but so close. Inflammopharmacology 2023;31:37–56. doi: https://doi.org/10.1007/s10787-022-01125-5.

[26] Zhang M, Tang Z. Therapeutic potential of natural molecules against Alzheimer's disease via SIRT1 modulation. Biomed Pharmacother 2023;161:114474. doi: https://doi.org/10.1016/j.biopha.2023.114474.

[27] Suzuki M, Ikeda A, Bartlett JD. Sirt1 overexpression suppresses fluoride-induced p53 acetylation to alleviate fluoride toxicity in ameloblasts responsible for enamel formation. Arch Toxicol 2018;92:1283–93. doi: https://doi.org/10.1007/s00204-017-2135-2.

[28] Dong, S.; Yang, Y.; He, B.; Xu, Z.; Zhou, Z.; Wang, J.; Chen, C.; Chen, Q. Effect of sodium fluoride on reproductive function through regulating reproductive hormone level and circulating SIRT1 in female rats. *Biol Trace Elem Res* 2022: Online ahead of print. doi:10.1007/s12011-022-03283-7.

[29] Li W, Dong S, Chen Q, Chen C, Dong Z. Selenium may suppress peripheral blood mononuclear cell apoptosis by modulating HSP70 and regulate levels of SIRT1 through reproductive hormone secretion and oxidant stress in women suffering fluorosis. Eur J Pharmacol 2020;878:173098. doi: https://doi.org/10.1016/j.ejphar.2020.173098.
[30] Mishra P, Mittal AK, Kalonia H, Madan S, Ghosh S, Sinha JK, et al. SIRT1 promotes neuronal fortification in neurodegenerative diseases through attenuation of pathological hallmarks and enhancement of cellular lifespan. Curr Neuropharmacol 2021;19:1019–37. doi: https://doi.org/10.2174/1570159X18666200729111744.
[31] Chen HH, Zhang YX, Lv JL, Liu YY, Guo JY, Zhao L, et al. Role of sirtuins in metabolic disease-related renal injury. Biomed Pharmacother 2023;161:114417. doi: https://doi.org/10.1016/j.biopha.2023.114417.
[32] Lin X, Fu B, Xiong Y, Xu S, Liu J, Zaky MY, et al. Folic acid ameliorates the declining quality of sodium fluoride-exposed mouse oocytes through the Sirt1/Sod2 pathway. Aging Dis 2022;13:1471–87. doi: https://doi.org/10.14336/AD.2022.0217.
[33] Fang J, Wu H, Zhang J, Mao S, Shi H, Yu D, et al. A reduced form of nicotinamide riboside protects the cochlea against aminoglycoside-induced ototoxicity by SIRT1 activation. Biomed Pharmacother 2022;150:113071. doi: https://doi.org/10.1016/j.biopha.2022.113071.
[34] Gu X, Wang Z, Gao J, Han D, Zhang L, Chen P, et al. SIRT1 suppresses p53-dependent apoptosis by modulation of p21 in osteoblast-like MC3T3-E1 cells exposed to fluoride. Toxicol In Vitro 2019;57:28–38. doi: https://doi.org/10.1016/j.tiv.2019.02.006.
[35] Wang H, Hao W, Yang L, Yan P, Wei S. Preconditioning with procyanidin B2 protects MAC-T cells against heat exposure-induced mitochondrial dysfunction and inflammation. Mol Immunol 2022;147:126–35. doi: https://doi.org/10.1016/j.molimm.2022.05.001.
[36] Cui Z, Zhao X, Amevor FK, Du X, Wang Y, Li D, et al. Therapeutic application of quercetin in aging-related diseases: SIRT1 as a potential mechanism. Front Immunol 2022;13:943321. doi: https://doi.org/10.3389/fimmu.2022.943321.
[37] Xu H, Liu YY, Li LS, Liu YS. Sirtuins at the crossroads between nitochondrial quality control and neurodegenerative diseases: structure, regulation, modifications, and modulators. Aging Dis 2023;14:794–824. doi: https://doi.org/10.14336/AD.2022.1123.
[38] Hyun DH, Lee J. A new insight into an alternative therapeutic approach to restore redox homeostasis and functional mitochondria in neurodegenerative diseases. Antioxidants (Basel) 2021;11:7. doi: https://doi.org/10.3390/antiox11010007.
[39] Zhang J, He Z, Fedorova J, Logan C, Bates L, Davitt K, et al. Alterations in mitochondrial dynamics with age-related Sirtuin1/Sirtuin3 deficiency impair cardiomyocyte contractility. Aging Cell 2021;20:e13419.
[40] Zheng M, Bai Y, Sun X, Fu R, Liu L, Liu M, et al. Resveratrol reestablishes mitochondrial quality control in myocardial ischemia/reperfusion injury through Sirt1/Sirt3-Mfn2-Parkin-PGC-1alpha pathway. Molecules 2022:27. doi: https://doi.org/10.3390/molecules27175545.
[41] Wan XM, Zheng C, Zhou XL. Puerarin prevents cadmium-induced mitochondrial fission in AML-12 cells via Sirt1-dependent pathway. Ecotoxicol Environ Saf 2022;248:114302. doi: https://doi.org/10.1016/j.ecoenv.2022.114302.
[42] Romanello V, Sandri M. Implications of mitochondrial fusion and fission in skeletal muscle mass and health. Semin Cell Dev Biol 2023;143:46–53. doi: https://doi.org/10.1016/j.semcdb.2022.02.011.
[43] Ashrafizadeh M, Zarrabi A, Mostafavi E, Aref AR, Sethi G, Wang L, et al. Non-coding RNA-based regulation of inflammation. Semin Immunol 2022:101606. doi: https://doi.org/10.1016/j.smim.2022.101606.
[44] Ouyang T, Qin Y, Luo K, Han X, Yu C, Zhang A, et al. miR-486-3p regulates CyclinD1 and promotes fluoride-induced osteoblast proliferation and activation. Environ Toxicol 2021;36:1817–28. doi: https://doi.org/10.1002/tox.23302.
[45] Li D, Zhao Q, Xie L, Wang C, Tian Z, Tang H, et al. Fluoride impairs mitochondrial translation by targeting miR-221-3p/c-Fos/RMND1 axis contributing to neurodevelopment defects. Sci Total Environ 2023;869:161738. doi: https://doi.org/10.1016/j.scitotenv.2023.161738.
[46] Abdolahi S, Zare-Chahoki A, Noorbakhsh F, Gorji A. A review of molecular interplay between neurotrophins and miRNAs in neuropsychological disorders. Mol Neurobiol 2022;59:6260–80. doi: https://doi.org/10.1007/s12035-022-02966-5.
[47] Guiot J, Henket M, Remacle C, Cambier M, Struman I, Winandy M, et al. Systematic review of overlapping microRNA patterns in COVID-19 and idiopathic pulmonary fibrosis. Respir Res 2023;24:112. doi: https://doi.org/10.1186/s12931-023-02413-6.
[48] Qu Y, Zhang J, Zhang J, Xiao W. MiR-708-3p alleviates inflammation and myocardial injury after myocardial infarction by suppressing ADAM17 expression. Inflammation 2021;44:1083–95. doi: https://doi.org/10.1007/s10753-020-01404-9.
[49] Lee JW, Guan W, Han S, Hong DK, Kim LS, Kim H. MicroRNA-708-3p mediates metastasis and chemoresistance through inhibition of epithelial-to-mesenchymal transition in breast cancer. Cancer Sci 2018;109:1404–13. doi: https://doi.org/10.1111/cas.13588.
[50] Liu B, Li R, Zhang J, Meng C, Zhang J, Song X, et al. MicroRNA-708-3p as a potential therapeutic target via the ADAM17-GATA/STAT3 axis in idiopathic pulmonary fibrosis. Exp Mol Med 2018;50:e465.
[51] R. Wang Y. Feng H. Xu H. Huang S. Zhao Y. Wang et al. Synergistic effects of miR-708-5p and miR-708-3p accelerate the progression of osteoporosis J Int Med Res 48 2020 300060520978015 10.1177/0300060520978015.
[52] Scheper M, Iyer A, Anink JJ, Mesarosova L, Mills JD, Aronica E. Dysregulation of miR-543 in Parkinson's disease: Impact on the neuroprotective gene SIRT1. Neuropathol Appl Neurobiol 2023;49:e12864.
[53] Liu T, Ma X, Ouyang T, Chen H, Xiao Y, Huang Y, et al. Efficacy of 5-aminolevulinic acid-based photodynamic therapy against keloid compromised by downregulation of SIRT1-SIRT3-SOD2-mROS dependent autophagy pathway. Redox Biol 2019;20:195–203. doi: https://doi.org/10.1016/j.redox.2018.10.011.
[54] Zhang J, Wang H, Slotabec L, Cheng F, Tan Y, Li J. Alterations of SIRT1/SIRT3 subcellular distribution in aging undermine cardiometabolic homeostasis during ischemia and reperfusion. Aging Cell 2023;22:e13930.
[55] Wang D, Cao L, Pan S, Wang G, Wang L, Cao N, et al. Sirt3-mediated mitochondrial dysfunction is involved in fluoride-induced cognitive deficits. Food Chem Toxicol 2021;158:112665. doi: https://doi.org/10.1016/j.fct.2021.112665.